Published in final edited form as:

FASEB J. 2022 May ; 36(5): e22275. doi:10.1096/fj.202200160R.

ClC-K2 Cl^- channel allows identification of A- and B-type of intercalated cells in split-opened collecting ducts

Kyrylo Pyrshev[1], **Naghmeh Hassanzadeh Khayyat**[1], **Anna Stavniichuk**[1], **Viktor N. Tomilin**[1], **Oleg Zaika**[1], **Nirupama Ramkumar**[2], **Oleh Pochynyuk**[1]

[1]Department of Integrative Biology and Pharmacology, the University of Texas Health Science Center at Houston, Houston, Texas, USA

[2]Division of Nephrology and Hypertension, University of Utah Health, Salt Lake City, Utah, USA

Abstract

The collecting duct is a highly adaptive terminal part of the nephron, which is essential for maintaining systemic homeostasis. Principal and intercalated cells perform different physiological tasks and exhibit distinctive morphology. However, acid-secreting A- and base secreting B-type of intercalated cells cannot be easily separated in functional studies. We used BCECF-sensitive intracellular pH (pH_i) measurements in split-opened collecting ducts followed by immunofluorescent microscopy in WT and intercalated cell-specific ClC-K2$^{-/-}$ mice to demonstrate that ClC-K2 inhibition enables to distinguish signals from A- and B-intercalated cells. We show that ClC-K2 Cl^- channel is expressed on the basolateral side of intercalated cells, where it governs Cl^--dependent H^+/HCO_3^- transport. ClC-K2 blocker, NPPB, caused acidification or alkalization in different subpopulations of intercalated cells in WT but not ClC-K2$^{-/-}$ mice. Immunofluorescent assessment of the same collecting ducts revealed that NPPB increased pH_i in AE1-positive A-type and decreased pH_i in pendrin-positive B-type of intercalated cells. Induction of metabolic acidosis led to a significantly augmented abundance and H^+ secretion in A-type and decreased proton transport in B-type of intercalated cells, whereas metabolic alkalosis caused the opposite changes in intercalated cell function, but did not substantially change their relative abundance. Overall, we show that inhibition of ClC-K2 can be employed to discriminate between A- and B-type of intercalated cells in split-opened collecting duct preparations. We further demonstrate that this method can be used to independently monitor changes in the functional status and abundance of A- and B-type in response to systemic acid/base stimuli.

Correspondence: Oleh Pochynyuk, Department of Integrative Biology and Pharmacology, University of Texas Health Science Center at Houston, 6431 Fannin, Houston, TX 77030, USA. Oleh.M.Pochynyuk@uth.tmc.edu.
Kyrylo Pyrshev and Naghmeh Hassanzadeh Khayyat contributed equally to this study.

AUTHOR CONTRIBUTIONS

Conceptualization: Oleh Pochynyuk; investigation: Kyrylo Pyrshev, Naghmeh Hassanzadeh Khayyat, Viktor N. Tomilin, Oleg Zaika, and Oleh Pochynyuk; formal analysis: Kyrylo Pyrshev, Naghmeh Hassanzadeh Khayyat, Oleg Zaika, Viktor N. Tomilin, and Oleh Pochynyuk; funding acquisition: Viktor N. Tomilin and Oleh Pochynyuk; provided materials: Nirupama Ramkumar; writing original draft: Oleh Pochynyuk; editing: Kyrylo Pyrshev, Naghmeh Hassanzadeh Khayyat, Oleg Zaika, Viktor N. Tomilin, Nirupama Ramkumar, and Oleh Pochynyuk.

DISCLOSURE

The authors declare that they have no conflict of interest with the contents of this article.

SUPPORTING INFORMATION

Additional supporting information may be found in the online version of the article at the publisher's website.

Keywords

acid–base disorders; AE1; intracellular pH; pendrin; V-ATPase

1 | INTRODUCTION

The collecting duct is known to play a critical role in maintaining whole body homeostasis by matching urinary excretion rate with perpetual day-to-day changes in water and electrolyte intake.[1–3] Indeed, inherited or acquired dysfunction of the collecting duct transport systems gives rise to a number of diseases, including Pseudohypoaldosteronism type I (PHA I), Liddle syndrome, nephrogenic diabetes insipidus, and distal renal tubule acidosis type I (dRTA type I) to name a few.[4–6] Collecting duct is the most heterogeneous segment of the renal nephron containing two electrically uncoupled cell types: principal and intercalated.[1,2] More abundant (up to 70% of total population) principal cells have relatively flat and polygonal shape and are largely involved in Na^+ and water reabsorption and K^+ secretion.[1] Intercalated cells mediate acid–base transport, Cl^- reabsorption, and K^+ secretion/reabsorption.[2] Intercalated cells are in general more round and darker due to high mitochondrial content.[7,8] They could be, to a certain degree of success, distinguished from principal cells even with a conventional light microscopy. Further studies demonstrated that intercalated cells are divided into two functionally distinct types. Acid secreting A-type is characterized by the presence of the H^+-ATPase on the apical membrane and the anion exchanger 1 (AE1, *Slc4a1*) on the basolateral side, whereas HCO_3^--secreting B-type expresses the anion exchanger pendrin (*Slc26a4*) on the apical membrane and H^+-ATPase basolaterally.[2,9] Despite quite distinct cellular ultrastructure and functional roles, A- and B-type cannot be visually discriminated thus requiring advanced imaging tools, such as electron or immunofluorescent microscopy.[7,10]

Isolated perfused cortical collecting ducts are capable of net secreting either H^+ or HCO_3^-,[11] which is consistent with the presence of both types of intercalated cells, thus enabling adaptation of the collecting duct to systemic pH stimuli. Of interest, the connecting tubule and cortical collecting duct also contain intercalated cells expressing H^+-ATPase and pendrin simultaneously on the apical side, the so-called non-A non-B-type.[12] While its exact physiological function is not defined, it is thought that non-A non-B might represent a transition pool to facilitate responses to systemic pH insults.[2] However, there is no consensus about the mechanism of adaptation. Thus, it was shown that chronic acid load led to increased total number of A-type of cells due to direct conversion of the polarity of B-type.[13–15] However, other studies concluded that neither metabolic nor respiratory acidosis were able to change the relative number of type A and type B cells in the cortical collecting duct, and the response was rather mediated by the increase in apical micro-projections and in the surface density of the apical membrane of type A cells.[16,17]

Secretion of H^+ or HCO_3^- by intercalated cells depends on Cl^- due to the presence of AE1 on the basolateral membrane of A-type and pendrin on the apical side in of B-type, respectively.[2] Removal of Cl^- from the luminal or basolateral sides elicited discrete changes in intracellular pH (pH_i) in acid- and base-secreting intercalated cells in perfused

collecting ducts.[14] This permits identification of a limited number of intercalated cells located closer to the sides of the perfused collecting duct. The accurate separation of fluorescence-based signals from individual cells within a perfused tubule is also not readily feasible and often requires expensive instrumentations. The development of a split-opened collecting duct technique[18] enables unambiguous separation of signals simultaneously from a large number of epithelial cells within a split-opened area using conventional wide-field fluorescent microscopy setup.[19] However, it comes at a price of inability to selectively change concentration of ions (and particularly Cl^-) on the apical and basolateral side to distinguish A- and B-type of intercalated cells.

ClC-K2 (ClC-Kb in humans) is a virtually kidney-specific Cl^- channel abundantly expressed on the basolateral membrane of the several distal nephron segments from the thick ascending limb to the medullary collecting duct where it is thought to be essential for mediating trans-cellular Cl^- reabsorption.[20–25] Loss-of-function mutations in the *Clcnkb* gene encoding ClC-Kb underlie the Bartter's syndrome type 3 causing hypotension, urinary salt wasting, hypokalemia and metabolic alkalosis,[26] which is likely to be mediated by diminished NaCl reabsorption in the thick ascending limb and the distal convoluted tubule.[25] On the contrary, gain-of-function polymorphism ClC-Kb^{T481S} in humans is associated with elevated blood pressure.[27,28] We and others have shown that ClC-K2 is the dominant Cl^- channel on the basolateral membrane of intercalated but not principal cells of the collecting duct.[29–32] However, little is known about the physiological roles of ClC-K2 in this segment.

Taking the selective pattern of ClC-K2 expression into consideration, namely basolateral membrane of intercalated cells, the current study examined the idea that ClC-K2 is essential for the Cl^--dependent acid–base transport and that manipulation with channel activity could be instrumental in discrimination of A- and B-type of intercalated cells in split-opened collecting ducts.

2 | METHODS

2.1 | Reagents

All chemicals and materials were from Sigma (St. Louis, MO, USA), VWR (Radnor, PA, USA), Fisher (Waltham, MA, USA), and Tocris (Ellisville, MO, USA) unless noted otherwise and were at least of reagent grade.

2.2 | Research animals

Animal use and welfare adhered to the NIH Guide for the Care and Use of Laboratory Animals following protocols reviewed and approved by the Animal Care and Use Committees of the University of Texas Health Science Center at Houston. Animals were maintained on standard rodent chow and have free access to tap water. To induce metabolic acidosis/alkalosis, animals were given water supplemented with 280 mM NH_4Cl + 0.5% sucrose (acid load) or 280 mM $KHCO_3$ + 0.5% sucrose (base load) for 3 days, respectively, as was described previously.[33]

For experiments, 6- to 10-week old C57Bl/6 (WT), ClC-$K2^{fl/fl}$, and ClC-$K2^{fl/fl}$ -B1 ATPase-cre male mice were used. ClC-$K2^{fl/fl}$ mice were developed by the NIH sponsored UC Davis

Mouse Biology Program (project # MBP-1181; MGI: 6152442). Specifically, exons 3–20 of the *Clcnkb* gene (Chromosome 4), encoding ClC-K2 were flanked with loxP sites (Figure S1A). The genotyping primers were 5′-TAAGAGAGAGTACACTGGAATGTCCTAGC and 5′-TATACGAAGTTATACGTGTCGACAACG (for detection of floxed allele at 409 bp); 5′-TAAGAGAGAGTACACTGGAATGTCCTAGC and ATGGCAGCTCTAGTGTGTATTTGGGTA (for detection of WT allele at 530 bp). Figure S1B shows the representative images of genotyping of ClC-K2$^{fl/WT}$ and ClC-K2$^{fl/fl}$. ClC-K2$^{fl/fl}$ mice were further crossed with ATP6V1B1 (ATPase-B1) -cre[34] to create intercalated cell knockout of ClC-K2. The genotyping primers for B1-cre were 5′-CCCTCTTCCCTTCTCCCTCCA and 5′-GCGAACATCTTCAGGTTCTGCGG to detect a product at 580 bp. Figure S1C shows the representative images of genotyping of ClC-K2$^{fl/WT}$ B1 ATPase-cre and ClC-K2$^{fl/fl}$ B1 ATPase-cre.

2.3 | Isolation and split opening of cortical collecting ducts

The procedure for isolation of the cortical collecting ducts from mouse kidneys suitable for fluorescent pH_i measurements closely followed the protocols previously published by our group.[19,35,36] Kidneys were cut into thin slices (<1 mm) with slices placed into an ice-cold bath solution containing (in mM): 150 NaCl, 5 KCl, 1 $CaCl_2$, 2 $MgCl_2$, 5 glucose and 10 HEPES (pH 7.35). Cortical collecting ducts were visually identified by their morphological features (pale color; coarse surface) and by their post-experimental staining with anti-AQP2, anti-AE1, and anti-pendrin. The collecting ducts were mechanically isolated from kidney slices by micro-dissection using watchmaker forceps under a stereomicroscope. Isolated collecting ducts were attached to 5 × 5 mm cover glasses coated with poly-L-lysine. A cover-glass containing a collecting duct was placed in a perfusion chamber mounted on an inverted Nikon Eclipse Ti-S microscope and perfused with bath solution at room temperature. Cortical collecting ducts were further split-opened with two sharpened micropipettes, controlled with different micromanipulators, to reliably monitor pH_i signals from individual cells within a monolayer. The collecting ducts were used within 2 h of isolation.

2.4 | Intracellular pH measurements

Split-opened cortical collecting ducts were loaded with 2′,7′-Bis-(2-Carboxyethyl)-5-(and-6)-Carboxyfluoresce in (BCECF) by incubation with 15 μM BCECF-AM acetoxymethyl ester in the bath solution for 40 min at room temperature followed by a washout with the bath solution for additional 10 min. Collecting ducts were placed in an open-top imaging study chamber (RC-26GLP; Warner Instruments, Hamden, CT, USA) with a bottom coverslip viewing window and the chamber attached to the microscope stage of a Nikon Ti-S Wide-Field Fluorescence Imaging System (Nikon Instruments, Melville, NY, USA) integrated with Lambda XL light source (Sutter Instrument, Novato, CA, USA) and QIClick 1.4 megapixel monochrome CCD camera (QImaging, Surrey, BC, Canada) via NIS Elements 4.3 Imaging Software (Nikon Instruments, Melville, NY, USA). Cells were imaged with a 40X Nikon Super Fluor objective and regions of interest (ROIs) were drawn for individual cells. The BCECF fluorescence intensity ratio was determined by excitation at 495 and 440 nm and calculating the ratio of the emission intensities at 520 nm every 5 s. Experiments were performed under permanent perfusion of a solution containing (in mM): 150 NaCl, 5 KCl, 1 $CaCl_2$, 2 $MgCl_2$, 5 glucose and 10 HEPES at 1.5 ml/min rate.

Minor BCECF bleaching during the timeline of experiments was corrected. The changes in the ratio were converted into changes in pH_i by performing a calibration in high K^+ solutions (145 mM KCl) with predefined pH (6.0, 7.0, and 8.0, adjusted by HCl and KOH, respectively) in the presence of 15 μM nigericin, as was originally described.[37] In average, 6 individual collecting ducts (30–50 cells in each) from three mice were used for each experimental set. For intracellular acidification, a solution containing (in mM): 40 NH_4Cl 110 NaCl, 5 KCl, 1 $CaCl_2$, 2 $MgCl_2$, 5 glucose and 10 HEPES was applied to the recording chamber for 2 min. The rate of recovery after acidification was calculated as a linear slope of the initial pH_i recovery rate from the lowest pH_i values for each cell after removal of the acidification pulse, as we did previously.[33,36]

2.4.1 | Immunofluorescent microscopy—Following pH_i measurements, split-opened collecting ducts were fixed with 10% neutral buffered formalin (AzerScientific, Morgantown, PA, USA; Cat. # PFNBF240) for 15 min at room temperature. After fixation, the samples were permeabilized by addition of 1% SDS (Sigma-Aldrich, St. Louis, MO, USA; Cat. # L4390) in phosphate buffer solution (PBS) for 10 min and washed in PBS 2 times for 10 min. Nonspecific staining was blocked with 10% normal goat serum (Novus Biologicals™, Centennial, CO, USA; Cat. # NBP223475) in PBS for 1 h at room temperature. The samples were incubated overnight at +4°C in dark with anti-AQP2 antibodies (1:4000, Alomone Labs, Israel; Cat. # AQP2-002) or anti-AE1 antibodies (1:200, Invitrogen, Rockford, IL, USA; Cat. # PA5-114893) or anti-pendrin antibodies (1:250, Invitrogen, Rockford, IL, USA; Cat. # PA5-42060), washed with PBS, and incubated with Alexa 594 secondary antibodies (1:1000 Invitrogen; Cat. # A11012). For double staining, the samples were further blocked with 10% normal rabbit serum (Novus Biologicals™, Centennial, CO, USA; Cat. # NBP171681) for 30 min and incubated with anti-ClC-K primary antibodies (1:500, Alomone Labs, Israel; Cat. # ACL-004) conjugated with Alexa 594 F(ab')2 secondary antibodies (1:1000 Jackson Immunoresearch, West Grove, PA, USA Cat. # 111-587-003) for 60 min at 37°C. After washing with PBS (2 times for 5 min), the samples were stained with 4′,6-diamidino-2-phenylindole (DAPI) (300 nM concentration, MilliporeSigma™, Calbiochem, San Diego, CA, USA; Cat. # 5.08741.0001) to visualize nuclei. The samples were mounted with Fluoromount mounting media (Thermo Scientific, Pittsburg, PA, USA).

Freshly isolated kidneys were decapsulated and placed into cryo-tubes with embedding medium (Andwin Scientific Tissue-Tek™ CRYO-OCT Compound 4583, Torrance, CA, USA; Cat. # 14-373-65). The kidneys were flash-frozen in liquid nitrogen for 3–5 min. Transverse cut 6 μm thick sections were made on CM 1850 cryostat (Leica, Buffalo Grove, IL, USA). The sections were allowed to warm to room temperature, washed three times in phosphate buffer saline (PBS) and fixed with 10% neutral buffered formalin for 15 min. Following the three times washing for 10 min, kidney sections were permeabilized with 0.1% Triton x100 (Sigma-Aldrich, St. Louis, MO, USA; Cat. # 56H0850) for 10 min following washout with PBS and blockade of nonspecific binding with 10% normal goat serum for an hour at room temperature. Sections were further incubated overnight at +4°C with anti-AQP2 (1:4000, Alomone Labs, Israel; Cat. # AQP2-002) conjugated with Alexa 488 F(ab') secondary antibodies (1:1000 Invitrogen, Eugene, OR, USA; Cat.

A1182668) followed by washing with PBS for 20 min at room temperature. After blockade of nonspecific binding with 10% normal rabbit serum for 30 min at room temperature, kidney sections were incubated with anti-ClC-K antibodies (1:500, Alomone Labs, Israel; Cat. # ACL-004) conjugated with Alexa 594 F(ab')2 secondary antibodies (1:1000 Jackson Immunoresearch, West Grove, PA, USA; Cat. # 111-587-003) for 90 min at 37°C. After washing with PBS for 20 min at room temperature, nuclei were stained with DAPI (0.5 μg/ml) for 10 min at room temperature. The samples were mounted with Fluoromount mounting media (Thermo Scientific, Pittsburg, PA, USA). Specificity of employed antibodies was verified by the absence of any fluorescent signal upon their pre-incubation with respective blocking peptide and, for the case of ClC-K, the absence of fluorescent signal in AQP2-negative intercalated cells of ClC-K2$^{fl/fl}$ B1 ATPase-cre mice (Figure S6). The labeled kidney sections or split-opened collecting ducts were imaged with a Nikon A1R confocal microscope, as we did similarly before.[38,39] In brief, samples were excited with 405, 488, and/or 561 nm laser diodes and emission captured with a 16-bit Cool SNAP HQ^2 camera (Photometrics) interfaced to a PC running NIS elements software.

2.5 | Data analysis

All summarized data are reported as mean ± SEM. Statistical comparisons were made using one-way ANOVA with post-hoc Tukey test or one-way repeated measures ANOVA with post hoc Bonferroni test. p value less than .05 was considered significant.

3 | RESULTS

3.1 | Functional expression of ClC-K2 Cl^- channel in intercalated but not principal cells of the collecting duct

It was previously documented that ClC-K2 channel is expressed on the basolateral side in the distal nephron from the thick ascending limb to the inner medullary collecting duct.[23] However, there is a drastic switch in the expression pattern of ClC-K2 in the collecting duct compared to the upstream segments. As exemplified in Figure 1A, ClC-K2-reporting signal is detected in AQP2-negative intercalated cells of the collecting duct, whereas it is present in all cells of the distal convoluted tubule and the thick ascending limb (see Figure S2 for panoramic view). Such a mosaic expression argues that ClC-K2 is well-suited to control acid–base transport in the collecting duct (Figure 1B). Thus, we next assessed the functional consequences of ClC-K2 inhibition with 5-Nitro-2-(3-phenylpropylamino) benzoic acid (NPPB, 100 μM) on pH_i in split-opened cortical collecting ducts loaded with pH-sensitive dye, BCECF (Figure 2A). We subsequently probed the same collecting ducts with anti-AQP2 antibodies to sort out the signals from principal (AQP2-positive) and intercalated (AQP2-negative) cells (Figure 2A, bottom panel). As summarized in Figure 2B, NPPB had no effect on pH_i in principal cells, which is consistent with the lack of ClC-K2 expression in this cell type (Figure 1A). Importantly, we detected two opposite responses to ClC-K2 inhibition in intercalated cells. NPPB induced a notable acidification in the majority of intercalated cells (Figure 2A and another example in Figure S3, yellow arrows), whereas it led to alkalization in the remaining minority in intercalated cells (Figures 2A and S3, white arrows). These two populations were termed as ICs− and ICs+, respectively. The

actions of NPPB on pH_i were reversible upon washout (Figure 2B). Of note, ICs− had a considerably higher baseline pH_i than ICs+: 7.03 ± 0.02 versus 6.86 ± 0.02.

NPPB could also block other Cl^- channels, most notably CFTR, which was shown to be expressed in the intercalated cells.[40] However, application of a specific CFTR inhibitor, $CFTR_{in}$-172 (5 μM), did not induce any acute changes in pH_i in both intercalated and principal cells (Figure S4). Moreover, neither blockade of Na^+ conducting pathway with amiloride (2 μM,[41]) nor K^+ conductance with Ba^{2+} (30 μM,[42]) affected pH_i in all types of collecting duct cells (Figure S5). This argues against putative contribution of indirect secondary mechanisms in NPPB-induced changes in pH_i. Altogether, our results suggest that ClC-K2 is functional specifically in intercalated but not principal cells of the collecting duct. Inhibition of ClC-K2 with NPPB causes acute bidirectional changes in pH_i, which could indicate the opposite responses from the acid-secreting A-type and base-secreting B-type of intercalated cells.

3.2 | ClC-K2 deletion abolishes NPPB-dependent changes in pH_i in intercalated cells

We next verified that NPPB-dependent changes in pH_i in intercalated cells were solely mediated by ClC-K2 inhibition. For this, we created intercalated cell-specific ClC-K2 knockout by crossing ClC-$K2^{fl/fl}$ with ATP6V1B1 (B1 ATPase)-cre (Figure S1, see Methods for additional details). As shown in the representative images of split-opened collecting ducts, ClC-K2 expression is evident in AQP2-negative intercalated cells of ClC-$K2^{fl/fl}$ (Figure 3A), but not in ClC-$K2^{fl/fl}$ B1 ATPase-cre mice (Figure 3B). Consistently, ClC-K2-reporting signal was absent in intercalated cells of the knockout, but present outside the collecting duct in both cortical and medullary kidney sections (Figure S6). NPPB application led to acute acidification in ICs− and alkalization in ICs+ of ClC-$K2^{fl/fl}$ (Figure 3C) with responses being indistinguishable from those observed in WT (C57Bl/6) mice (Figures 2B and 3E). In contrast, NPPB elicited only marginally detectable changes in pH_i in intercalated cells from ClC-$K2^{fl/fl}$ B1 ATPase-cre mice (Figure 3D). The magnitude of the responses was less than 10% of the respective values seen in WT and ClC-$K2^{fl/fl}$ (Figure 3E). These results demonstrate that NPPB can be used as a reliable and specific tool to block ClC-K2 activity in intercalated cells of the collecting duct. The residual minor effects observed in ClC-$K2^{fl/fl}$ B1 ATPase-cre mice are most likely caused by incomplete deletion of the channel with cre-lox technology.

3.3 | ClC-K2 inhibition induces opposite responses in A- and B-type of intercalated cells

Our next set of experiments tested the hypothesis that bidirectional changes in pH_i upon ClC-K2 inhibition reflect responses from acid-secreting A- and base-secreting B-type of intercalated cells. Upon measurements of NPPB-induced changes in pH_i, split-opened collecting ducts were probed with antibodies for AE1, a specific marker of A-type of intercalated cells (Figure 4A). The individual responses from AE1-positive and AE1-negative intercalated cells are shown in Figure 4B left and right panels, respectively. As summarized in the pie chart graphs in Figure 4B, over 95% of ICs+ were positive for AE1, and almost 80% of ICs− did not exhibit a notable AE1-reporting signal. We next similarly probed split-opened collecting ducts with antibodies for pendrin, a selective marker of B-type intercalated cells. As shown in Figure 4C, over 91% of ICs− were pendrin positive,

and almost 80% of ICs+ were pendrin negative. Overall, we concluded that inhibition of ClC-K2 with NPPB leads to pH_i alkalization in the overwhelming majority of A-type and to acidification specifically in B-type, thus being a highly reliable and feasible tool for discrimination between intercalated cell types in split-opened collecting duct preparations.

3.4 | Using ClC-K2 inhibition to monitor adaptation of the collecting duct to metabolic acidosis/alkalosis

We next implemented this method to independently monitor function of A- and B-intercalated cells in the cortical collecting duct. As shown in Figure 5A, isotonic application of NH_4Cl (40 mM for 2 min) caused an alkalization followed by an acute acidification upon NH_4Cl removal. This allows quantification of the rate of apical H^+ extrusion by A-type of intercalated cells and basolateral H^+ extrusion by B-type of intercalated cells upon pH_i recovery to the basal level. Followed the recovery, A- and B-type were distinguished by their responses to NPPB: alkalization and acidification, respectively (Figure 5A). Finally, the collecting duct was fixed and probed with anti-AQP2 antibodies to separate signals from principal cells and to verify that NPPB elicited pH_i changes exclusively in intercalated cells (Figure 5A). The averaged time course of pH_i changes for each cell type is shown in Figure 5B, left panel. B-type was more abundant, making up to 65% of the total population of intercalated cells (Figure 5B, middle panel). The rate of recovery after NH_4Cl-induced acidification was not statistically different for A- (0.58 ± 0.08 ΔpH/min) and B-type (0.47 ± 0.04 ΔpH/min). However, both values were much greater than that observed in principal cells (0.061 ± 0.003 ΔpH/min), as expected. Deletion of ClC-K2 in intercalated cells substantially decreased the recovery after acidification in both A-type (by 45%) and B-type (by 78%), when compared to WT (Figure S7). In this case, the types of AQP2-negative cells were distinguished by their residual minor responses to NPPB, similar to that shown in Figure 3D. Overall, this strongly suggests a critical role of ClC-K2 in controlling acid–base transport in the collecting duct.

We next used this experimental design to monitor changes in the function of A- and B-type of intercalated cells of WT mice in response to systemic acid–base stimuli. First, mice were kept on ammonium water (280 mM) for 3 days to induce metabolic acidosis, as previously described.[33] This treatment did not affect the recovery rate after acidification in principal cells (0.054 ± 0.002 ΔpH/min). In contrast, we observed a notable acceleration of the recovery in A-type: 0.84 ± 0.09 ΔpH/min, and deceleration in B-type: 0.27 ± 0.02 ΔpH/min (Figure 5C). Moreover, there was a drastic shift in intercalated cell population with A-type becoming dominant: 57.7% versus 42.3% for B-type (Figure 5C, middle panel). We similarly kept mice on high bicarbonate (280 mM) water for 3 days to promote metabolic alkalosis. Again, the recovery rate after acidification was not substantially different in principal cells (0.043 ± 0.002 ΔpH/min), when compared to control condition. Systemic base load modestly augmented the recovery rate in B-type (0.56 ± 0.08 ΔpH/min), but caused a dramatic decrease in A-type to 0.24 ± 0.05 ΔpH/min (Figure 5D). However, we did not detect changes in the relative abundance in A- and B-type (38.3% and 61.7%; Figure 5D, middle panel), when compared to the control condition in Figure 5A. Finally, both systemic acid and base loads caused a small increase in the total population of intercalated cells from 34.5% to 37.2% and 39.4%, respectively (Figure 5B–D). Overall, our functional studies

demonstrate that adaptation of the cortical collecting duct to metabolic acidosis/alkalosis is a multicomponent process including both augmentation of function in the respective intercalated cell type, as well as changes in the relative abundance, specifically for A-type.

We have next tested whether systemic acidification/alkalization also affects ClC-K2-dependent changes in pH_i in intercalated cells. Inhibition of ClC-K2 with NPPB (100 μM) induced greater pH_i changes in A-type (Figure 6A), but elicited diminished responses in B-type (Figure 6B) of intercalated cells in mice subjected to acid load. Conversely, NPPB-induced responses were augmented in B-type (Figure 6B) and decreased in A-type (Figure 6A) in mice after systemic base load. As summarized in Figure 6C, NPPB-dependent changes in pH_i in A-type were 0.20 ± 0.01, 0.26 ± 0.01, and 0.14 ± 0.01 in the control, after acid, and base load, respectively. In B-type, NPPB application changed pH_i by −0.23 ± 0.02 (control), −0.13 ± 0.01 (acidification), and −0.29 ± 0.01 (alkalization). We similarly observed a notable increase in the abundance of A-type from 42.47% to 59.14% of the total intercalated cell population in response to metabolic acidosis but only a small increase in B-type cell population in response to metabolic alkalosis in this set of experiments (Figure 6D).

4 | DISCUSSION

In this study, we provided first direct evidence of the functional significance of ClC-K2 channel in regulation of acid–base transport in the collecting duct. Using fluorescent, pharmacological, and genetic tools, we showed that ClC-K2 is functionally expressed in both types of intercalated cells but not in principal cells. Moreover, ClC-K2 inhibition with NPPB led to intracellular alkalization in A-type but acidification in B-type (Figure 7), which can be employed to reliably discriminate between different types of intercalated cells in split-opened collecting duct preparations. We show that this method is instrumental to independently monitor function/abundance of A- and B-type of intercalated cells in response to systemic acid–base stimuli. Specifically, we detected a drastic increase in A-type cell population and augmented H^+ secretion as well as reduced abundance and functional activity of B-cells in response to metabolic acidosis. Conversely, metabolic alkalosis decreased the rate of H^+ secretion in A-type and stimulated activity of B-type, while it did not substantially alter their relative abundance (Figure 7). The changes in the rate of acid–base transport were also associated with respective increases/decreases of NPPB-induced changes in pH_i in A- and B-type strongly suggesting the direct contribution of ClC-K2 in governing the adaptation to systemic pH stimuli.

The index “K” in ClC-K2 and its very close homologue ClC-K1 emphasize their virtually kidney specific localization,[20,21] with inner ear being the only other notable site of their expression.[22,43] Approximately 90% identity of the secondary structures between ClC-K1 and ClC-K2 drastically complicates the development of specific antibodies and blockers. To this end, studies in the knockout mice were beneficial to uncover the pattern of expression of these channels in renal tissue. Thus, ClC-K1 seems to be exclusively expressed in the thin ascending limb.[23,44,45] In contrast, ClC-K2 is found in the thick ascending limb, distal convoluted tubule, and the collecting duct.[23,25,45] Consistently, we show that the deletion of ClC-K2 in intercalated cells prevents any specific staining with ClC-K antibodies (Figures

3A,B and S6) and abolishes pH_i responses to ClC-K2 inhibition (Figure 3C–E). We and others previously showed that Cl^- permeable 10 pS channel is present on the basolateral membrane of the distal convoluted and collecting duct intercalated cells of WT but not in mice with global ClC-K2 knockout.[25,29,30,32,46,47] Altogether, the cumulative evidence suggests that ClC-K2 and not ClC-K1 is the dominant basolateral Cl^- pathway in the collecting duct intercalated cells.

It has been shown that numerous mutations in ClC-Kb (which is the name of ClC-K2 in humans) cause Bartter's syndrome type 3 leading to hypotension, urinary salt wasting, hypokalemia, and metabolic alkalosis.[26,48] Mice with global ClC-K2 deletion exhibit all the major symptoms of Bartter's syndrome with hypovolemia being largely attributed to the disrupted NaCl reabsorption in the thick ascending limb and the distal convoluted tubule.[25] At the same time, it is currently unknown whether ClC-K2 also contributes to salt reabsorption in the collecting duct. Indeed, ClC-K2 in tandem with the apical Cl^-/HCO_3^- exchanger, pendrin, could mediate trans-cellular Cl^- reabsorption in the B-type of intercalated cells of the collecting duct,[9,49] although the direct evidence is still missing. In addition, it is reasonable to propose that the observed metabolic alkalosis in Bartter's patients and ClC-$K2^{-/-}$ mice could be, at least partially, caused by the impaired HCO_3^- secretion by B-type intercalated cells considering compromised basolateral Cl^- exit due to ClC-K2 deficiency. Consistently, we found that ClC-K2 deletion decreases the functional activity (i.e., recovery after acidification) by 78% in B-type, but only by 45% in A-type (Figure S7). Future studies are necessary to test this possibility.

We recognize that the ClC-K2 inhibitor, NPPB,[46] has very poor specificity and is known to inhibit other Cl^- channels and even mildly block anion exchangers.[50] To our advantage, we found that the off-target effects of NPPB are minimal in the collecting ducts. First, NPPB had no effect in principal cells (Figure 2B), which do not express ClC-K2 (Figures 1A and 2). Second, selective inhibition of CFTR Cl^- channel, which was shown to be present in intercalated cells,[40] did not reproduce the actions of NPPB on pH_i (Figure S4). Third, selective deletion of ClC-K2 in intercalated cells decreased NPPB-induced responses by more than 90% (Figure 3C–E). Thus, we posit with a high degree of confidence that NPPB is a reliable tool to monitor ClC-K2 activity in the collecting duct.

One might think that ClC-K2 blockade with NPPB would increase intracellular Cl^- levels in both A- and B-type of intercalated cells, thus leading to similar changes in pH_i. However, the opposite pH_i response to ClC-K2 inhibition in A- and B-type of intercalated cells was the most reproducible observation, as exemplified in the Figures showing actual pH_i changes in split-opened collecting ducts and summary graphs comparing these changes under different physiological conditions. These experimental results would be the most consistent with predominant blockade of the basolateral conductance in response to NPPB application, rather than with overall changes in intracellular Cl^-. In this case, inhibition of the basolateral Cl^- recycling (i.e., the tandem of ClC-K2 and AE1) would interfere with HCO_3^- extrusion in A-type of cells (IC+), whereas activity of the apical V-ATPase will increase pH_i levels by secreting H^+, as is observed (Figure 2B). The increase in pH_i will be limited due to the overabundance of intracellular HCO_3^-. Furthermore, inhibition of the basolateral conductance (i.e., both ClC-K2 and V-ATPase) would interfere with basolateral

H^+ exit and pH_i levels would initially decrease due to activity of the apical pendrin in B cells. However, an increase in intracellular Cl^- (due to ClC-K2 inhibition) is known to inhibit pendrin, resulting in a gradual restoration of pH_i back to the original levels. This is exactly what we observed in B-type (IC−) of intercalated cells. Along with this concept, removal of NPPB would also unblock V-ATPase thus resulting in an overshoot in pH_i observed in these cells (Figures 2–4), until ClC-K2-mediated reduction of intracellular Cl^- restores the function of pendrin. While we do not have direct proof of the concept that ClC-K2 activity is central for determining the basolateral conductance of intercalated cells in the collecting duct, we found that ClC-K2 deletion inhibits the basolateral H^+ exit more strongly in B-type than the apical H^+ secretion in A-type (Figure S7).

The major finding of this study is that ClC-K2 can be used to distinguish/identify A- and B-type of intercalated cells in split-opened collecting ducts. Thus, we found that ClC-K2 inhibition led to discrete and opposite pH_i changes in subpopulations of intercalated cells (Figure 2). We reasonably hypothesized that these bidirectional changes reflect responses from A- and B-type of intercalated cells. Consistently, removal of Cl^- in bath solution was shown to induce acidification in B-type and alkalization in A-type of intercalated cells in perfused collecting duct.[14] Using post-experimental staining with a specific A- and B-type markers, AE1 and pendrin, we further demonstrated that over 90% of intercalated cells that respond to ClC-K2 inhibition with intracellular alkalization are AE1 positive and with acidification are pendrin positive (Figure 4). It is worth noting that the magnitude of pH_i changes is comparable in both cell types (Figure 3E) likely indicating similar ClC-K2 functional activity and its role in regulation of acid–base transport in A- and B-type. The remaining minority of intercalated cells, which responded to ClC-K2 inhibition in an “unconventional” manner, could represent transition intermediary types.[51] For example, the non-A non-B type of intercalated cells is well described in the connecting tubule and the cortical collecting duct.[12] If the expression of V-ATPase is higher than that of pendrin, this non-A non-B cell would operate as an acid secreting A-type, despite it also being identified as pendrin positive and vice versa. While our NPPB-based method cannot distinguish between these transitional intercalated cell subtypes, it has necessary precision to inform about the overall function of a particular intercalated cell. Simply put, it allows unequivocal conclusion of whether this is an acid- or base-secreting cell, which is directly relevant to the integral renal ability to regulate urinary pH.

The classical work of Burg and Atkins[11] demonstrated that perfused cortical collecting duct reabsorb HCO_3^- (i.e., secrete H^+) in rats treated with ammonium water and secrete HCO_3^-, when animals are stressed with alkali. Our method brings this observation to a new level by allowing to independently quantify changes in the acid–base transport in A- and B-type and also to detect changes in their relative abundance in response to systemic acidosis and alkalosis (Figure 5). Specifically, we assessed the recovery after acidification with ammonium pulse in individual cells of different types. In the control, there were no significant differences in the apical and basolateral H^+ transport in A- and B-type, respectively. Metabolic acidosis after NH_4Cl induced a marked augmentation of H^+ secretion by the collecting duct. This was manifested as an accelerated recovery rate in A-type and an impaired recovery in B-type (Figure 5C). This is in agreement with reported reduction in the apical surface and pendrin expression in B-type and an increased

V-ATPase and AE1 expression in A-type during metabolic acidosis.[52] High-throughput analysis of cells in the split-opened preparation also allows detection of changes in the relative abundance of cell types in response to a treatment. While several studies showed an increase in the number of H^+-secreting cells and even conversion of some HCO_3^--secreting cells into H^+-secreting cells in a hensin-dependent manner, when isolated collecting ducts were perfused with acidic pH for 3 h,[13–15] other studies found no change in the percentage of alpha intercalated cells in response to metabolic and respiratory acidosis.[16,17] We detected more B-type than A-type at the baseline in two independent set of experiments (Figures 5 and 6). This is in agreement with previous report that 46% of intercalated cells of the cortical collecting duct express apical H^+-ATPase and basolateral AE1, thus being A-type.[53] In contrast, this pattern was reversed in the cortical collecting ducts from NH_4Cl-loaded mice (Figures 5C and 6D). Thus, our results support the view about increased A/B type ratio in metabolic acidosis, although we do not have any evidence in support of direct conversion between cell types. It is also quite possible that pendrin-positive B-type of cells would operate as acid-secreting cells after V-ATPase translocation to the apical membrane in response to metabolic acidosis. Of interest, experimentally induced metabolic alkalosis led to opposite but not symmetrical changes in A- and B-type of cells. We revealed a modestly increased basolateral H^+ extrusion in B-type and substantially decreased apical H^+ secretion in A-type (Figure 5D). However, this did not affect the A/B cell type ratio in one set of experiments (Figure 5D) and only mildly increased B-type abundance in another (Figure 6E). Importantly, we also found that metabolic acidosis and alkalosis significantly affected the magnitude of the respective NPPB-induced changes in pH_i in A- and B-type of cells (Figure 6). This provides an additional evidence that ClC-K2 is an important component of the collecting duct adaptation to systemic pH stimuli. Further studies are necessary to uncover the molecular details of this mechanism.

In conclusion, our study identifies a critical role of the basolateral ClC-K2 Cl^- channel in governing acid–base transport by the collecting duct intercalated cells. Furthermore, we show that ClC-K2 blockade with NPPB serves as an accurate and relatively easy-to-perform tool allowing discrimination between A- and B-type of intercalated cells in split-opened collecting duct preparations. Finally, we demonstrate that this ClC-K2-based method can be successfully used to detect changes in the functional status as well as abundance of intercalated cell types in response to metabolic acidosis and alkalosis. We propose that inhibition of ClC-K2 with NPPB (or another more specific antagonist when developed) could serve as a convenient tool to independently monitor function of A- and B-type of intercalated cells in normal physiology as well as during inherited or acquired acid–base disorders.

Supplementary Material

Refer to Web version on PubMed Central for supplementary material.

ACKNOWLEDGMENTS

We condemn Russian invasion to Ukraine on 02/24/2022 in the strongest possible way! We urge all countries and free people of the World to stand together with Ukraine to stop the barbaric genocide of civil Ukrainian people and children.

We thank Anna Zaika for editorial suggestion and proofreading of the manuscript. Raoul Nelson (University of Utah Health) is recognized for the development of ATP6V1B1 (ATPase-B1)-cre mice.

Funding information

This research was supported by NIH-NIDDK DK095029, DK117865, AHA EIA35260097 (to O. Pochynyuk), and AHA-19CDA34660148 (to V. N. Tomilin)

DATA AVAILABILITY STATEMENT

The data that support the findings of this study are available in the methods and/or Supporting Information of this article.

REFERENCES

1. Pearce D, Soundararajan R, Trimpert C, Kashlan OB, Deen PM, Kohan DE. Collecting duct principal cell transport processes and their regulation. Clin J Am Soc Nephrol. 2015;10:135–146. [PubMed: 24875192]
2. Roy A, Al-bataineh MM, Pastor-Soler NM. Collecting duct intercalated cell function and regulation. Clin J Am Soc Nephrol. 2015;10:305–324. [PubMed: 25632105]
3. Staruschenko A Regulation of transport in the connecting tubule and cortical collecting duct. Compr Physiol. 2012;2:1541–1584. [PubMed: 23227301]
4. Schild L The ENaC channel as the primary determinant of two human diseases: Liddle syndrome and pseudohypoaldosteronism. Nephrologie. 1996;17:395–400. [PubMed: 8987044]
5. Sands JM, Bichet DG, American College of Physicians; American Physiological Society. Nephrogenic diabetes insipidus. Ann Intern Med. 2006;144:186–194. [PubMed: 16461963]
6. Alper SL. Genetic diseases of acid-base transporters. Annu Rev Physiol. 2002;64:899–923. [PubMed: 11826292]
7. Madsen KM, Tisher CC. Structural-functional relationship along the distal nephron. Am J Physiol. 1986;250:F1–F15.
8. Rice WL, Van Hoek AN, Paunescu TG, et al. High resolution helium ion scanning microscopy of the rat kidney. PLoS One. 2013;8:e57051. [PubMed: 23505418]
9. Wall SM, Verlander JW, Romero CA. The renal physiology of pendrin-positive intercalated cells. Physiol Rev. 2020;100:1119–1147. [PubMed: 32347156]
10. Pham TD, Verlander JW, Wang Y, et al. Aldosterone regulates pendrin and epithelial sodium channel activity through intercalated cell mineralocorticoid receptor-dependent and -independent mechanisms over a wide range in serum potassium. J Am Soc Nephrol. 2020;31:483–499. [PubMed: 32054691]
11. Atkins JL, Burg MB. Bicarbonate transport by isolated perfused rat collecting ducts. Am J Physiol. 1985;249:F485–F489. [PubMed: 4051002]
12. Kim YH, Kwon TH, Frische S, et al. Immunocytochemical localization of pendrin in intercalated cell subtypes in rat and mouse kidney. Am J Physiol Renal Physiol. 2002;283:F744–F754. [PubMed: 12217866]
13. Schwartz GJ, Barasch J, Al-Awqati Q. Plasticity of functional epithelial polarity. Nature. 1985;318:368–371. [PubMed: 2415824]
14. Schwartz GJ, Tsuruoka S, Vijayakumar S, Petrovic S, Mian A, Al-Awqati Q. Acid incubation reverses the polarity of intercalated cell transporters, an effect mediated by hensin. J Clin Investig. 2002;109:89–99. [PubMed: 11781354]
15. Tsuruoka S, Schwartz GJ. Adaptation of rabbit cortical collecting duct HCO3- transport to metabolic acidosis in vitro. J Clin Investig. 1996;97:1076–1084. [PubMed: 8613531]
16. Verlander JW, Madsen KM, Tisher CC. Axial distribution of band 3-positive intercalated cells in the collecting duct of control and ammonium chloride-loaded rabbits. Kidney Int Suppl. 1996;57:S137–S147. [PubMed: 8941935]

17. Verlander JW, Madsen KM, Tisher CC. Effect of acute respiratory acidosis on two populations of intercalated cells in rat cortical collecting duct. Am J Physiol. 1987;253:F1142–F1156. [PubMed: 3425724]
18. Palmer LG, Frindt G. Amiloride-sensitive Na channels from the apical membrane of the rat cortical collecting tubule. Proc Natl Acad Sci USA. 1986;83:2767–2770. [PubMed: 2422661]
19. Mamenko M, Zaika O, O'Neil RG, Pochynyuk O. Ca^{2+} imaging as a tool to assess TRP channel function in murine distal nephrons. Methods Mol Biol. 2013;998:371–384. [PubMed: 23529445]
20. Kieferle S, Fong P, Bens M, Vandewalle A, Jentsch TJ. Two highly homologous members of the ClC chloride channel family in both rat and human kidney. Proc Natl Acad Sci USA. 1994;91:6943–6947. [PubMed: 8041726]
21. Uchida S, Sasaki S, Furukawa T, et al. Molecular cloning of a chloride channel that is regulated by dehydration and expressed predominantly in kidney medulla. J Biol Chem. 1993;268:3821–3824. [PubMed: 7680033]
22. Estevez R, Boettger T, Stein V, et al. Barttin is a Cl− channel beta-subunit crucial for renal Cl− reabsorption and inner ear K+ secretion. Nature. 2001;414:558–561. [PubMed: 11734858]
23. Kobayashi K, Uchida S, Mizutani S, Sasaki S, Marumo F. Intrarenal and cellular localization of CLC-K2 protein in the mouse kidney. J Am Soc Nephrol. 2001;12:1327–1334. [PubMed: 11423561]
24. Adachi S, Uchida S, Ito H, et al. Two isoforms of a chloride channel predominantly expressed in thick ascending limb of Henle's loop and collecting ducts of rat kidney. J Biol Chem. 1994;269:17677–17683. [PubMed: 8021279]
25. Hennings JC, Andrini O, Picard N, et al. The ClC-K2 chloride channel is critical for salt handling in the distal nephron. J Am Soc Nephrol. 2017;28:209–217. [PubMed: 27335120]
26. Simon DB, Bindra RS, Mansfield TA, et al. Mutations in the chloride channel gene, CLCNKB, cause Bartter's syndrome type III. Nat Genet. 1997;17:171–178. [PubMed: 9326936]
27. Jeck N, Waldegger P, Doroszewicz J, Seyberth H, Waldegger S. A common sequence variation of the CLCNKB gene strongly activates ClC-Kb chloride channel activity. Kidney Int. 2004;65:190–197. [PubMed: 14675050]
28. Sile S, Velez DR, Gillani NB, et al. CLCNKB-T481S and essential hypertension in a Ghanaian population. J Hypertens. 2009;27:298–304. [PubMed: 19226700]
29. Nissant A, Paulais M, Lachheb S, Lourdel S, Teulon J. Similar chloride channels in the connecting tubule and cortical collecting duct of the mouse kidney. Am J Physiol Renal Physiol. 2006;290:F1421–F1429. [PubMed: 16403836]
30. Tomilin VN, Zaika O, Subramanya AR, Pochynyuk O. Dietary K(+) and Cl(−) independently regulate basolateral conductance in principal and intercalated cells of the collecting duct. Pflugers Arch. 2018;470:339–353. [PubMed: 29134279]
31. Khayyat NH, Zaika O, Tomilin VN, Pyrshev K, Pochynyuk O. Angiotensin II increases activity of the ClC-K2 Cl(−) channel in collecting duct intercalated cells by stimulating production of reactive oxygen species. J Biol Chem. 2021;296:100347. [PubMed: 33524393]
32. Zaika O, Tomilin VN, Pochynyuk O. Adenosine inhibits the basolateral Cl(−) ClC-K2/b channel in collecting duct intercalated cells. Am J Physiol Renal Physiol. 2020;318:F870–F877. [PubMed: 31984792]
33. Zaidman NA, Tomilin VN, Hassanzadeh Khayyat N, et al. Adhesion-GPCR Gpr116 (ADGRF5) expression inhibits renal acid secretion. Proc Natl Acad Sci USA. 2020;117:26470–26481. [PubMed: 33004624]
34. Miller RL, Lucero OM, Riemondy KA, et al. The V-ATPase B1-subunit promoter drives expression of Cre recombinase in intercalated cells of the kidney. Kidney Int. 2009;75:435–439. [PubMed: 19052537]
35. Mironova E, Bugay V, Pochynyuk O, Staruschenko A, Stockand JD. Recording ion channels in isolated, split-opened tubules. Methods Mol Biol. 2013;998:341–353. [PubMed: 23529443]
36. Tomilin V, Mamenko M, Zaika O, Wingo CS, Pochynyuk O. TRPV4 deletion protects against hypokalemia during systemic K(+) deficiency. Am J Physiol Renal Physiol. 2019;316:F948–F956. [PubMed: 30838874]

37. Thomas JA, Buchsbaum RN, Zimniak A, Racker E. Intracellular pH measurements in Ehrlich ascites tumor cells utilizing spectroscopic probes generated in situ. Biochemistry. 1979;18:2210–2218. [PubMed: 36128]
38. Mamenko M, Dhande I, Tomilin V, et al. Defective store-operated calcium entry causes partial nephrogenic diabetes insipidus. J Am Soc Nephrol. 2016;27:2035–2048. [PubMed: 26574044]
39. Berrout J, Jin M, Mamenko M, Zaika O, Pochynyuk O, O'Neil RG. Function of TRPV4 as a mechanical transducer in flow-sensitive segments of the renal collecting duct system. J Biol Chem. 2012;287:8782–8791. [PubMed: 22298783]
40. Berg P, Svendsen SL, Sorensen MV, et al. Impaired renal HCO3 (−) excretion in cystic fibrosis. J Am Soc Nephrol. 2020;31:1711–1727. [PubMed: 32703846]
41. Canessa CM, Schild L, Buell G, et al. Amiloride-sensitive epithelial Na+ channel is made of three homologous subunits. Nature. 1994;367:463–467. [PubMed: 8107805]
42. Zaika O, Palygin O, Tomilin V, Mamenko M, Staruschenko A, Pochynyuk O. Insulin and IGF-1 activate Kir4.1/5.1 channels in cortical collecting duct principal cells to control basolateral membrane voltage. Am J Physiol Renal Physiol. 2016;310:F311–F321. [PubMed: 26632606]
43. Sage CL, Marcus DC. Immunolocalization of ClC-K chloride channel in strial marginal cells and vestibular dark cells. Hear Res. 2001;160:1–9. [PubMed: 11591484]
44. Matsumura Y, Uchida S, Kondo Y, et al. Overt nephrogenic diabetes insipidus in mice lacking the CLC-K1 chloride channel. Nat Genet. 1999;21:95–98. [PubMed: 9916798]
45. Limbutara K, Chou CL, Knepper MA. Quantitative proteomics of all 14 renal tubule segments in rat. J Am Soc Nephrol. 2020;31:1255–1266. [PubMed: 32358040]
46. Lourdel S, Paulais M, Marvao P, Nissant A, Teulon J. A chloride channel at the basolateral membrane of the distal-convoluted tubule: a candidate ClC-K channel. J Gen Physiol. 2003;121:287–300. [PubMed: 12668733]
47. Zaika O, Mamenko M, Boukelmoune N, Pochynyuk O. IGF-1 and insulin exert opposite actions on ClC-K2 activity in the cortical collecting ducts. Am J Physiol Renal Physiol. 2015;308:F39–F48. [PubMed: 25339702]
48. Andrini O, Keck M, Briones R, Lourdel S, Vargas-Poussou R, Teulon J. ClC-K chloride channels: emerging pathophysiology of Bartter syndrome type 3. Am J Physiol Renal Physiol. 2015;308:F1324–F1334. [PubMed: 25810436]
49. Zaika O, Tomilin V, Mamenko M, Bhalla V, Pochynyuk O. New perspective of ClC-Kb/2 Cl− channel physiology in the distal renal tubule. Am J Physiol Renal Physiol. 2016;310:F923–F930. [PubMed: 26792067]
50. Bernardinelli E, Costa R, Nofziger C, Paulmichl M, Dossena S. Effect of known inhibitors of ion transport on Pendrin (SLC26A4) activity in a human kidney cell line. Cell Physiol Biochem. 2016;38:1984–1998. [PubMed: 27161422]
51. Schuster VL. Function and regulation of collecting duct intercalated cells. Annu Rev Physiol. 1993;55:267–288. [PubMed: 8466177]
52. Purkerson JM, Tsuruoka S, Suter DZ, Nakamori A, Schwartz GJ. Adaptation to metabolic acidosis and its recovery are associated with changes in anion exchanger distribution and expression in the cortical collecting duct. Kidney Int. 2010;78:993–1005. [PubMed: 20592712]
53. Alper SL, Natale J, Gluck S, Lodish HF, Brown D. Subtypes of intercalated cells in rat kidney collecting duct defined by antibodies against erythroid band 3 and renal vacuolar H+-ATPase. Proc Natl Acad Sci USA. 1989;86:5429–5433. [PubMed: 2526338]

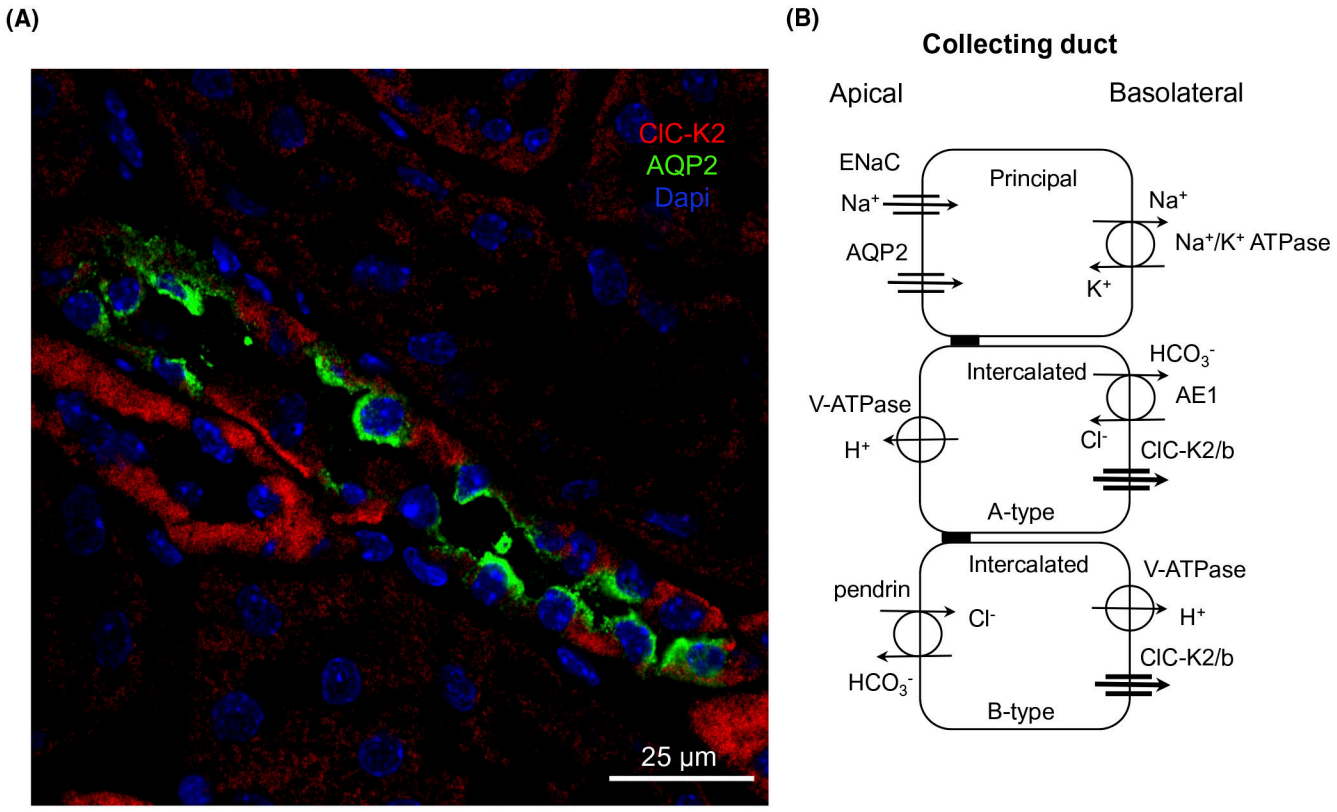

FIGURE 1.

ClC-K2 is expressed in intercalated but not principal cells of the collecting duct. (A) Representative high magnification confocal image depicting an individual cortical collecting duct probed with anti-AQP2 (pseudocolor green), anti-ClC-K2 (pseudocolor red), and Dapi (blue). (B) Schematic representation of heterogeneity of the cell types in the collecting duct depicting principal and both major types of intercalated cells. Principal cells express the epithelial Na^+ channel (ENaC) and aquaporin 2 (AQP2) on the apical membrane and Na^+/K^+ ATPase on the basolateral membrane. Intercalated acid secreting (A-type) cells express the proton pump V-ATPase on the apical and the anion exchanger 1 (AE1) on the basolateral membrane, respectively. The base secreting (B-type) intercalated cells express anion exchanger pendrin on the apical side and the proton pump V-ATPase on the basolateral side. The kidney-specific ClC-K2 Cl^- channel (highlighted in bold) is expressed on the basolateral membrane of both types of intercalated cells

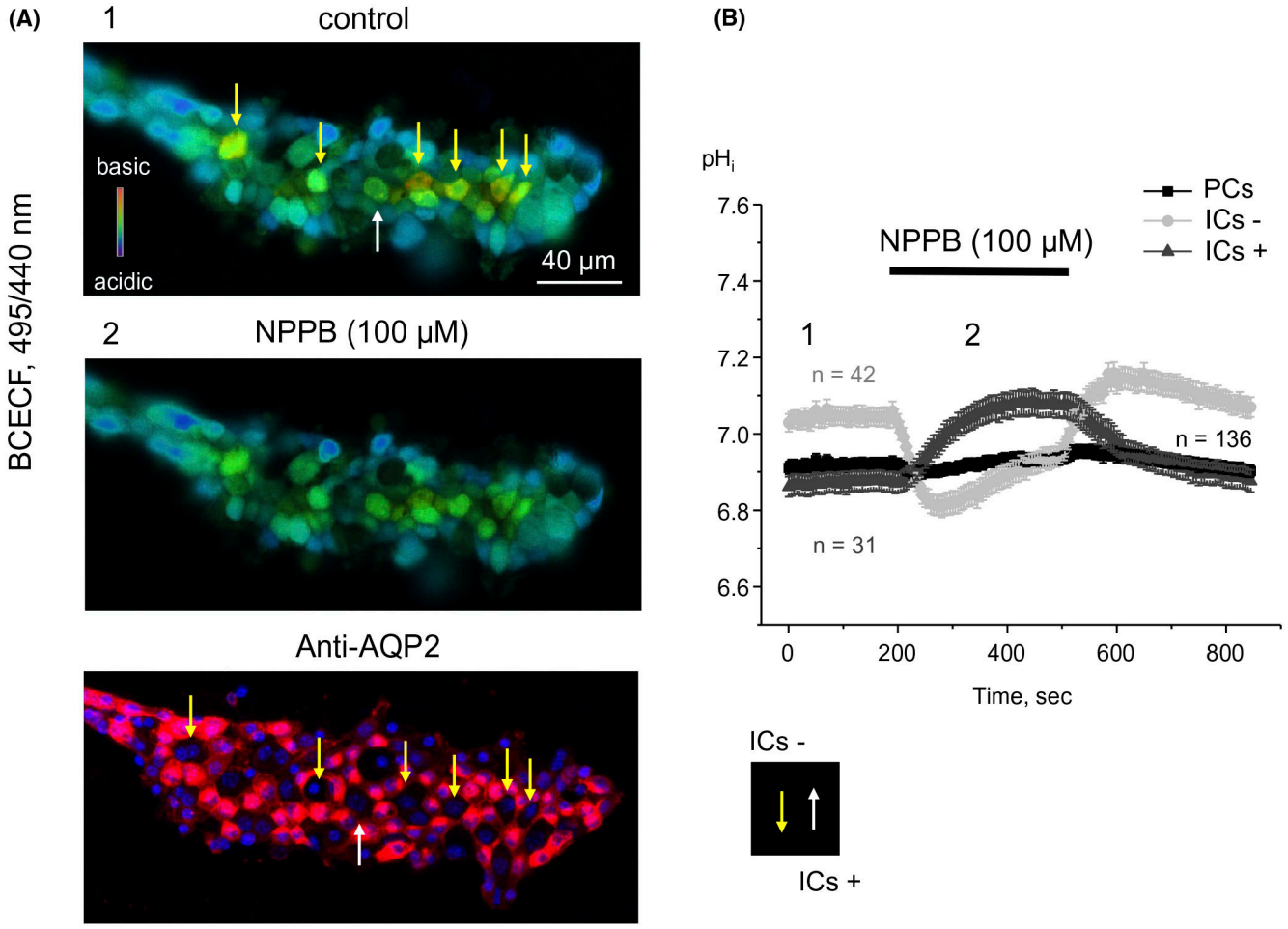

FIGURE 2.

Inhibition of ClC-K2 causes bidirectional changes of pH_i in intercalated cells of the collecting duct. (A) Representative pseudocolor images (blue—acidic and red—alkali) of intracellular pH (pH_i) in a split-opened cortical collecting duct loaded with pH-sensitive dye BCECF at the control (Time point 1) and upon application of the ClC-K2 blocker, 5-Nitro-2-(3-phenylpropylamino) benzoic acid (NPPB, 100 μM; Time point 2). Confocal micrograph of the same split-opened collecting duct probed with anti-AQP2 (pseudocolor red) is shown on the bottom. Nuclear Dapi staining is shown in pseudocolor blue. The examples of AQP2-negative intercalated cells responding to NPPB application with acidification (ICs−) and alkalization (ICs+) are shown with yellow and white arrows, respectively. (B) Summary graph of changes in pH_i in principal (black), ICs− (light gray) and IC+ (dark gray) in the control, upon application with NPPB (shown with a black bar on top), and following washout. The time points 1 (control) and 2 (NPPB) correspond to those shown in (A). Number of individual cells are shown for each group. Three different mice and six individual collecting ducts were used

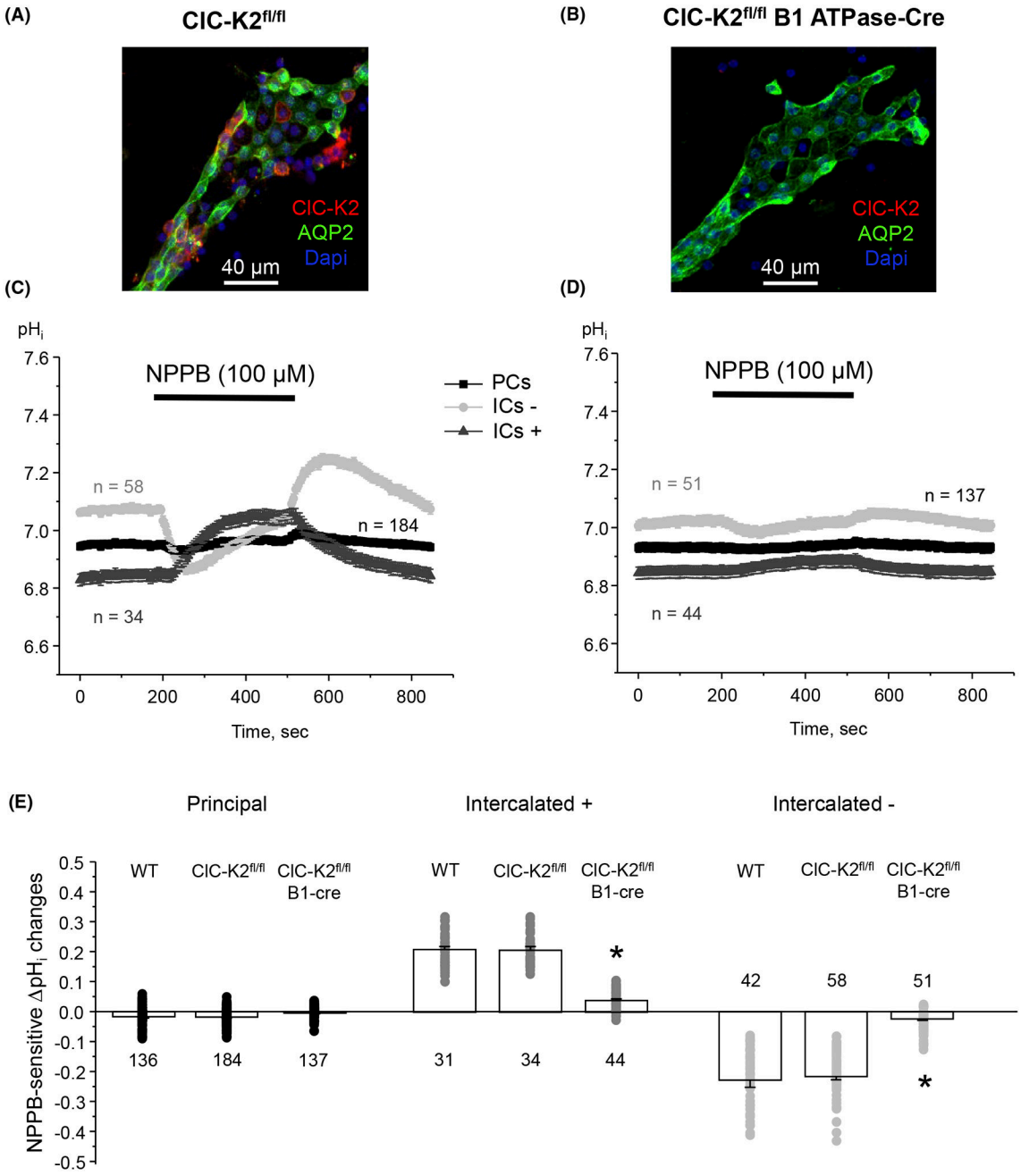

FIGURE 3.

Deletion of ClC-K2 in intercalated cells abolishes NPPB actions on pH_i. Representative confocal images of split-opened cortical collecting ducts from ClC-$K2^{fl/fl}$ (A) and ClC-$K2^{fl/fl}$ B1 ATPase-Cre (B) mice probed with anti-AQP2 (pseudocolor green) and anti-ClC-K (pseudocolor red). Nuclear Dapi staining is shown in blue. The time courses of changes in pH_i in principal (black), ICs− (light gray) and IC+ (dark gray) in the control, upon application with NPPB (shown with a black bar on top), and following washout in the collecting duct from ClC-$K2^{fl/fl}$ (C) and ClC-$K2^{fl/fl}$ B1 ATPase-Cre (D) mice. (E) Summary graph comparing NPPB-induced changes in pH_i in principal, ICs− (intercalated cells

responding with acidification), and ICs+ (intercalated cells responding with alkalization) in collecting ducts from WT, ClC-K2$^{fl/fl}$, and ClC-K2$^{fl/fl}$ B1 ATPase-Cre mice. *significant change ($p < .05$) versus WT. Three different mice and six individual collecting ducts were used for each experimental condition

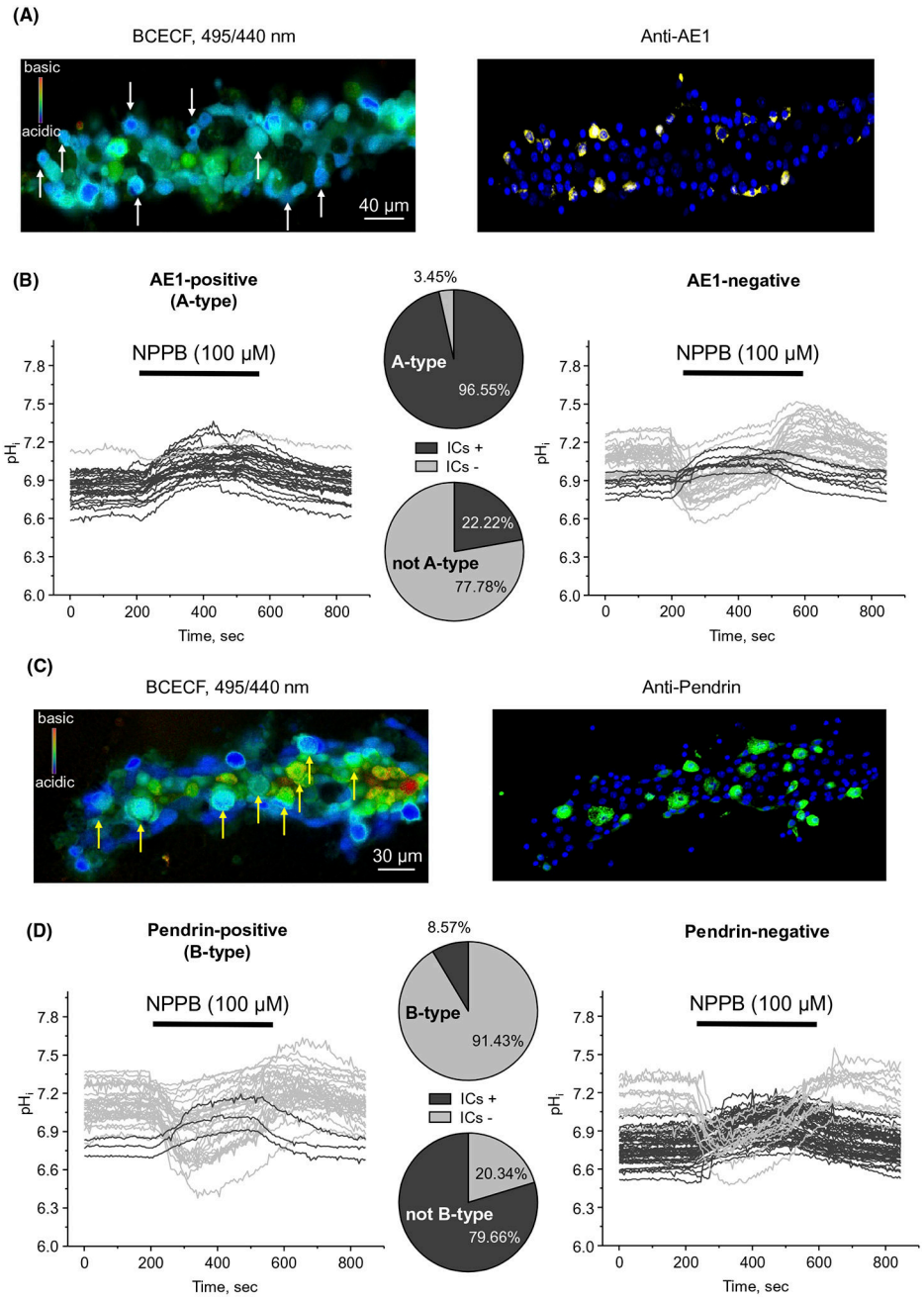

FIGURE 4.

Inhibition of ClC-K2 with NPPB elicits opposite changes in pH_i in A- and B-type of intercalated cells. (A) Representative pseudocolor image (blue—acidic and red—alkali) of intracellular pH (pH_i) in a split-opened cortical collecting duct loaded with pH-sensitive dye BCECF (left) and confocal image of the same collecting duct probed with anti-AE1 in pseudocolor yellow (right). Nuclear Dapi staining is shown in pseudocolor blue. Examples of AE1-positive intercalated cells (A-type) are shown with white arrows. (B) Time course of changes in pH_i in individual AE1-positive (left) and AE1-negative (right) intercalated cells in the control, upon application with NPPB (shown with a black bar on top), and following

washout. ICs+ (intercalated cells responding with alkalization) and ICs− (intercalated cells responding with acidification) are highlighted with dark gray and light gray, respectively. The pie chart graphs showing the prevalence of IC− and IC+ in AE1 positive (A-type) and AE1 negative of intercalated cells are shown in the middle. (C) Representative pseudocolor image (blue—acidic and red—alkali) of pH_i in a split-opened cortical collecting duct loaded with pH-sensitive dye BCECF (left) and confocal image of the same collecting duct probed with anti-pendrin in pseudocolor green (right). Nuclear Dapi staining is shown in pseudocolor blue. Examples of pendrin-positive intercalated cells (B-type) are shown with yellow arrows. (D) Time course of changes in pH_i in individual pendrin-positive (left) and pendrin-negative (right) intercalated cells in the control, upon application with NPPB (shown with a black bar on top), and following washout. ICs+ (intercalated cells responding with alkalization) and ICs− (intercalated cells responding with acidification) are highlighted with dark gray and light gray, respectively. The pie chart graphs showing the prevalence of IC− and IC+ in pendrin positive (B-type) and pendrin negative of intercalated cells are shown in the middle. Two different mice and four individual collecting ducts were used for each experimental condition of intercalated

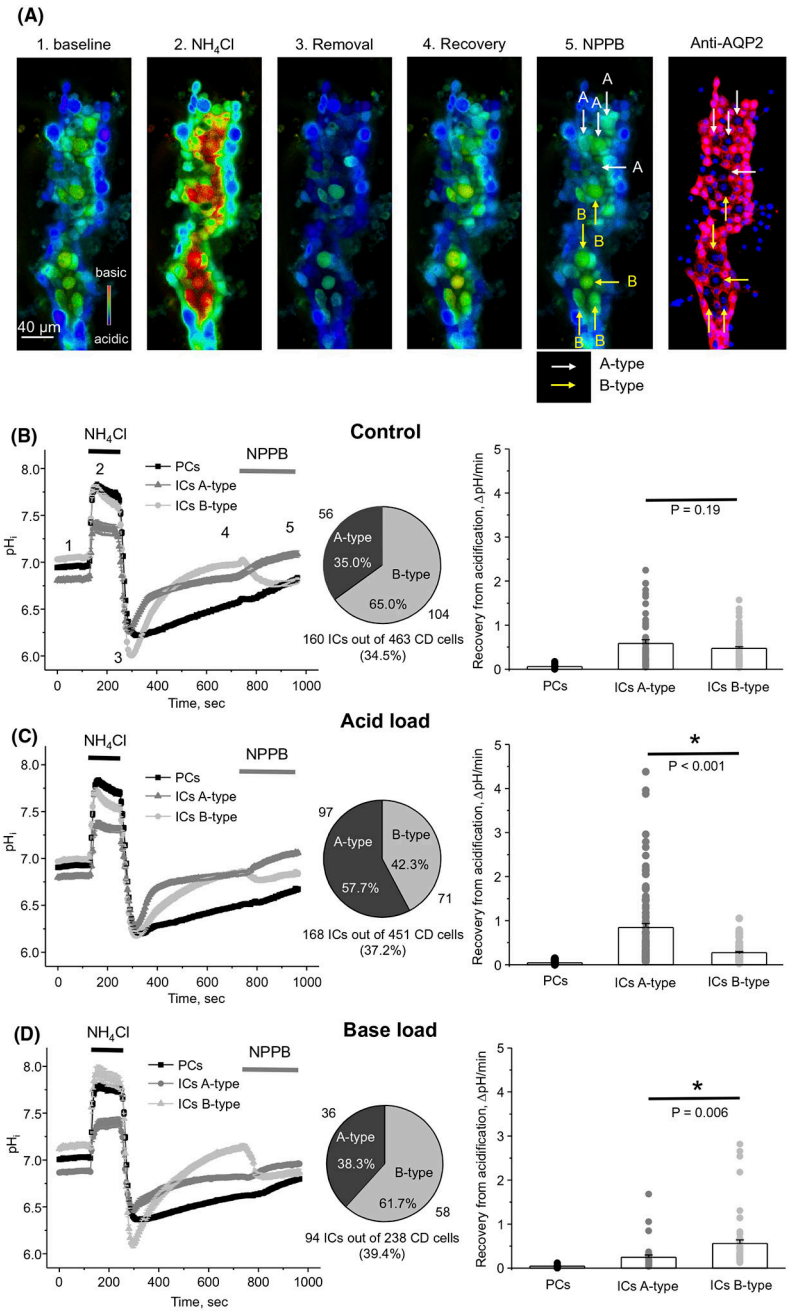

FIGURE 5.

Metabolic acidosis/alkalosis-induced changes in the function and relative expression of A- and B-type of intercalated cells. (A) Representative pseudocolor images (blue—acidic and red—alkali) of intracellular pH (pH_i) in a split-opened cortical collecting duct loaded with pH-sensitive dye BCECF at the baseline (1), upon application of 40 mM NH_4Cl (2), immediately after NH_4Cl removal (3), upon recovery to the baseline pH_i values (4), and following application on ClC-K2 blocker NPPB. Confocal micrograph of the same split-opened CD probed with anti-AQP2 (pseudocolor red) is shown on the right. Examples of A-type (responding with alkalization) and B-type (responding with acidification) of

intercalated cells are depicted with white and yellow arrows, respectively. Nuclear DAPI staining is shown in pseudocolor blue. (B) The left panel shows the summary graph comparing the time course of pH_i changes in principal (black), A-type (gray) and B-type (light gray) of intercalated cells upon application of 40 mM NH_4Cl (shown with a black bar on top) and NPPB (shown with a gray bar on top) in the cortical collecting ducts from control mice. The time points shown in (A) are marked as 1–5. The relative abundance of A- and B-type of intercalated cells as well as their actual numbers are shown as the pie chart graph in the middle. The right panel contains the summary graph of the recovery after acidification in principal cells, A- and B-type of intercalated cells. The rate was calculated for each individual cell (shown as dots) as a linear slope of the initial pH_i recovery from the lowest pH_i value after 40 mM NH_4Cl removal. (C) The left panel shows the summary graph comparing the time course of pH_i changes in principal (black), A-type (gray), and B-type (light gray) of intercalated cells upon application of 40 mM NH_4Cl (shown with a black bar on top) and NPPB (shown with a gray bar on top) in the cortical collecting ducts from acid-loaded mice treated with 280 mM NH_4Cl in drinking water for 3 days. The relative abundance of A- and B-type of intercalated cells as well as their actual numbers are shown as the pie chart graph in the middle. The right panel contains the summary graph of the recovery after acidification in principal cells, A-type and B-type of intercalated cells from the collecting ducts of acid-treated mice. The rate was calculated for each individual cell (shown as dots) as a linear slope of the initial pH_i recovery from the lowest pH_i value after 40 mM NH_4Cl removal. *significant decrease ($p < .05$) versus ICs A-type. (D) The left panel shows the summary graph comparing the time course of pH_i changes in principal (black), A-type (gray), and B-type (light gray) of intercalated cells upon application of 40 mM NH_4Cl (shown with a black bar on top) and NPPB (shown with a gray bar on top) in the cortical collecting ducts from base loaded mice treated with 280 mM $KHCO_3$ in drinking water for 3 days. The relative abundance of A- and B-type of intercalated cells as well as their actual numbers are shown as the pie chart graph in the middle. The right panel contains the summary graph of the recovery after acidification in principal cells, A-type and B-type of intercalated cells from the collecting ducts of base-treated mice. The rate was calculated for each individual cell (shown as dots) as a linear slope of the initial pH_i recovery from the lowest pH_i value after 40 mM NH_4Cl removal. *significant increase ($p < .05$) versus ICs A-type

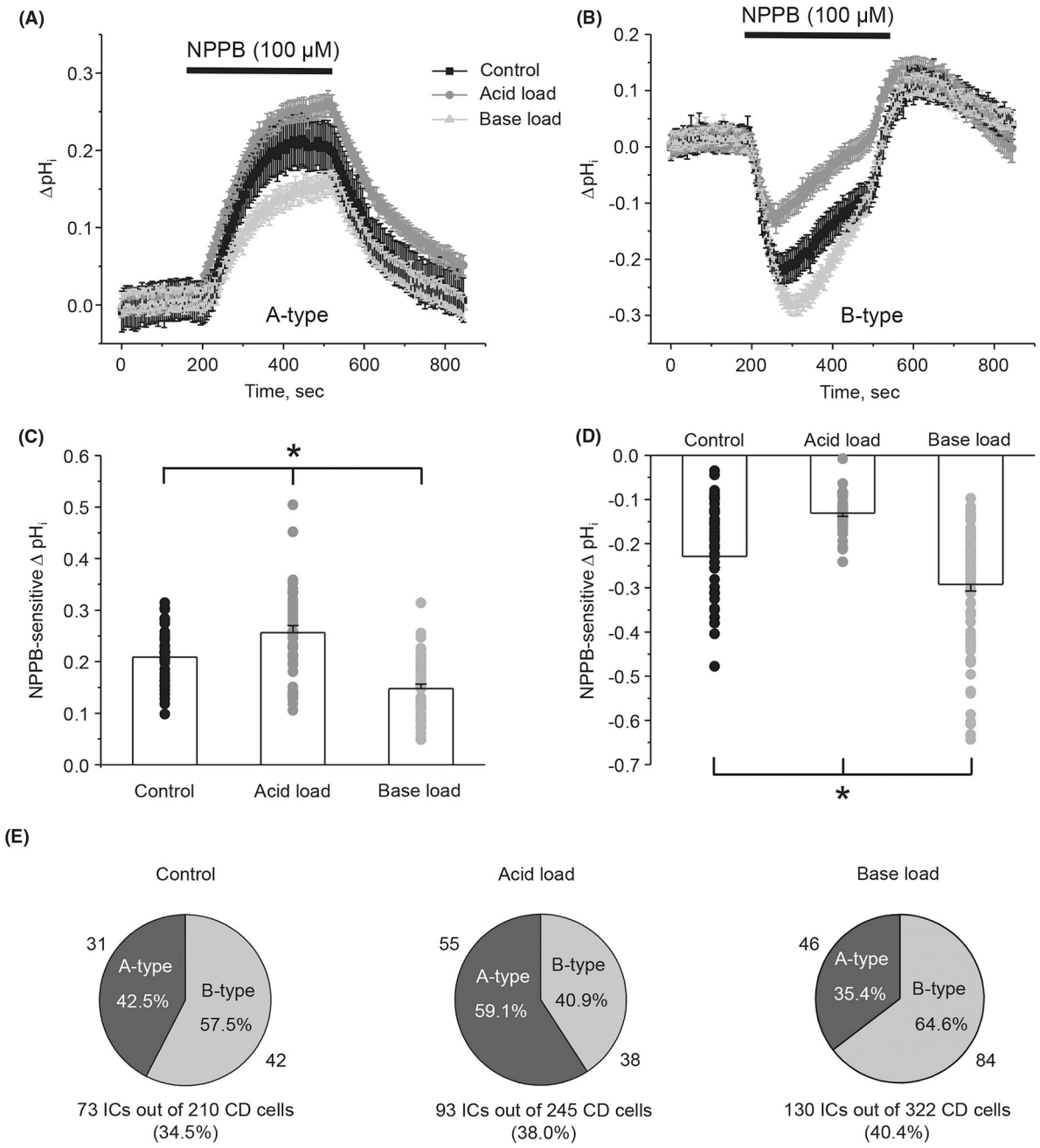

FIGURE 6.

Metabolic acidosis and alkalosis exhibit opposite effects on the magnitude of NPPB-induced pH_i changes in A- and B-type of intercalated cells. The time courses of changes in pH_i in A-type (A) and B-type (B) intercalated cells upon application NPPB (100 μM, shown with a black bar on top) in split-opened collecting duct from control (black), acid-loaded (gray), and base-loaded (light gray) mice. Mice were treated with 280 mM NH_4Cl and 280 mM $KHCO_3$ in drinking water for 3 days, respectively. Summary graphs comparing NPPB-induced changes in pH_i in A-type (C) and B-type (D) of intercalated cells in split-opened collecting ducts from control, acid-loaded, and base-loaded mice. Four different mice and

eight individual collecting ducts were used for each experimental condition. *significant difference ($p < .05$) versus respective control values. (E) Pie chart graphs of the relative abundance of A- and B-type of intercalated cells in collecting ducts of control, acid-loaded, and base-loaded mice. The actual numbers of A- and B-type of intercalated cells are shown for experimental condition

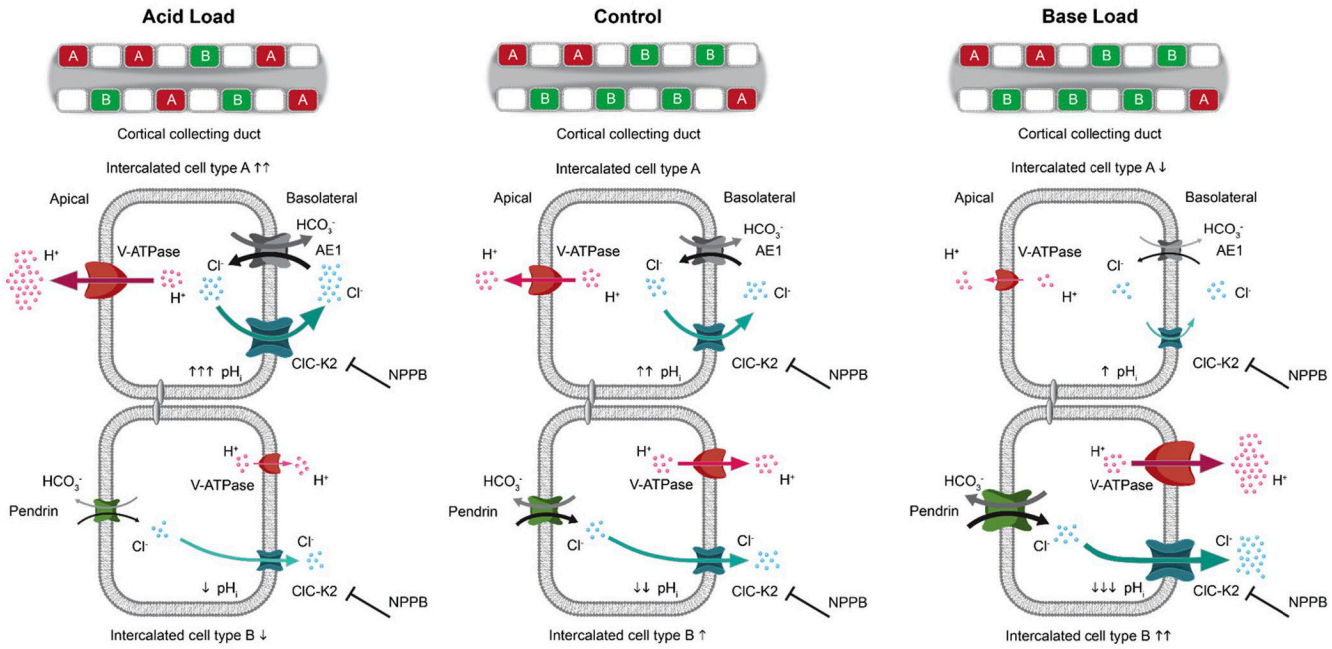

FIGURE 7.

Principal scheme of a role of ClC-K2 in regulation of acid–base transport in the collecting duct. The major molecular mechanisms of H^+ and HCO_3^- secretion by A- and B-type of intercalated cells in the control (middle), after acid load (right panel) and after base load (right panel). AE1—anion exchanger 1. The size of respective icons of transporting systems reflects their activity. The effects of ClC-K2 inhibition with NPPB on pH_i are shown with respective arrows. The upward direction indicates alkalization and downward direction reflects acidification. The number of arrows correlated with the magnitude of the respective changes in pH_i. The schematic representation of the relative abundance of A- and B-type of intercalated cells in the collecting duct in control and upon acid load is shown on the top